Energy spectra of superfluid turbulence in ^{3}He

Laurent Boué, Victor L'vov, Anna Pomyalov, and Itamar Procaccia
Department of Chemical Physics, The Weizmann Institute of Science, Rehovot 76100, Israel
(Received 28 December 2011; revised manuscript received 31 January 2012; published 6 March 2012)

In superfluid ^{3}He-B, turbulence is carried predominantly by the superfluid component. To explore the statistical properties of this quantum turbulence and its differences from the classical counterpart, we adopt the time-honored approach of shell models. Using this approach, we provide numerical simulations of a Sabra shell model that allows us to uncover the nature of the energy spectrum in the relevant hydrodynamic regimes. These results are in qualitative agreement with analytical expressions for the superfluid turbulent energy spectra that were found using a differential approximation for the energy flux.

DOI: 10.1103/PhysRevB.85.104502 PACS number(s): 67.30.hb, 47.37.+q

I. INTRODUCTION

Superfluids are known to display many spectacular properties, such as the fountain effect and rolling films, which are unique to quantum hydrodynamics. Ever since the discovery of superfluids, it was conjectured that their hydrodynamics can be described as two interpenetrating fluids with two different velocities v_s (superfluid component) and v_n (normal component).[1,2] The relative density of each component (ρ_s and ρ_n, respectively) depends on the temperature; this so-called "two-fluid" model was later developed very usefully by Landau.[2] In this model, the normal component is described by the Navier-Stokes equations and the superfluid part is modeled by the Euler equation. Accordingly, the inviscid supercomponent is characterized formally by an infinite Reynolds number: it is very easy for superfluids to become turbulent. Quantum mechanics plays an important role: unlike classical fluids where the circulation around the vortices is a statistical and dynamical variable, the properties of quantum vortices are tightly constrained by the laws of quantum mechanics. The circulation around a quantum vortex is quantized to integer values of a fundamental unit called the quantum of circulation $\kappa = 2\pi\hbar/m$, where m is the mass of a superfluid particle. Because of this, one can identify an additional typical length scale in quantum turbulence, referred to herewith as ℓ, which corresponds to the mean distance between quantum vortices.

At finite temperatures $T \neq 0$, the normal and superfluid components are coupled to each other via thermal excitations and the resulting dissipative force is called the mutual friction. This description is in qualitative variance with ordinary fluids and accordingly the question of how different classical and quantum turbulence are has emerged as a hot topic in the fluid mechanics community.[3,4] An important step in establishing a theory of quantum turbulence consists in developing a framework that describes the energy spectra of both the normal $E_n(k)$ and the superfluid $E_s(k)$ components. The work to achieve this goal is still developing, and there is a possibility that progress here might also shed some light on some long-standing classical turbulence problems.

Because of the high kinematic viscosity of ^{3}He (comparable to that of olive oil),[5] the normal component can usually be considered to be at rest with respect to the superfluid component with $v_n \ll v_s$. In such circumstances, we propose that the overall behavior of quantum turbulence is largely dominated by the superfluid velocity $\boldsymbol{v} \equiv \boldsymbol{v}_s$ component only.[6] Therefore, the description of the fluid motion can be reduced to the coarse-grained hydrodynamic equation for the superfluid velocity $\boldsymbol{v}(\boldsymbol{r},t)$, considered on length scales of the order of l, which are larger than intervortex distance ℓ:

$$\frac{\partial \boldsymbol{v}}{\partial t} + (\boldsymbol{v}\cdot\boldsymbol{\nabla})\,\boldsymbol{v} + \boldsymbol{\nabla}\mu = -\boldsymbol{D} + \boldsymbol{f}. \tag{1a}$$

Here, μ is the chemical potential, $\boldsymbol{f}(\boldsymbol{r},t)$ is a random force, which is introduced in order to mimic the energy injection that sustains turbulence; this force acts at the outer scale $l_0 \gg l \gg \ell$. The dissipative term $\boldsymbol{D}$ represents the effective mutual friction, which is the last remnant of the underlying but vanishingly small normal component. Throughout the paper, it should be kept in mind that the largest relevant wave vector is $k_{\max} = 1/\ell$; in other words, we restrict ourselves to the pure hydrodynamic regime of superfluid turbulence. In this case, the mutual friction can be approximated[7] as $\boldsymbol{D} \approx \alpha\,\boldsymbol{\omega}\times(\boldsymbol{\omega}\times\boldsymbol{v})/|\boldsymbol{\omega}|$. Here, α is the temperature-dependent dimensionless mutual friction parameter and $\boldsymbol{\omega} = \boldsymbol{\nabla}\times\boldsymbol{v}$ is the superfluid vorticity. This expression can be further simplified by averaging out the vectorial structure and recognizing that vorticity in hydrodynamic turbulence is dominated by the smallest possible eddies with $k \sim 1/\ell$. Because of their small size, these eddies also have very small turnover times. On the other hand, the superfluid velocity $\boldsymbol{v}$ is dominated by the largest eddies who, in turn, have a very long turnover time. This means that $\boldsymbol{\omega}$ and $\boldsymbol{v}$ can be considered as almost completely uncorrelated. In this case, we can replace $\boldsymbol{\omega}$ by its mean-square value and the dissipation term can be approximated by

$$\boldsymbol{D} \approx \Gamma\boldsymbol{v}, \tag{1b}$$

$$\Gamma \equiv \alpha\,\omega_{\mathrm{T}}\,, \quad \omega_{\mathrm{T}}^2 \equiv \langle|\boldsymbol{\omega}|^2\rangle \approx 2\int_{k_0}^{1/\ell} k^2 E(k)\,dk, \tag{2}$$

where $E(k)$ is the so-called one-dimensional (1D) energy spectrum, normalized such that the total energy density per unit mass is $E = \int E(k)dk$.

Our goal in the following is to analyze the *stationary* energy spectra of superfluid turbulence $E(k)$ at scales larger than the intervortex distance. This allows us to simplify further the problem by considering Γ in Eq. (1b) as a time-independent external parameter. Then, after finding $E(k)$ for a prescribed Γ, we can get the α corresponding to that Γ using Eq. (2). We will see that even after all these simplifications, the spectra found

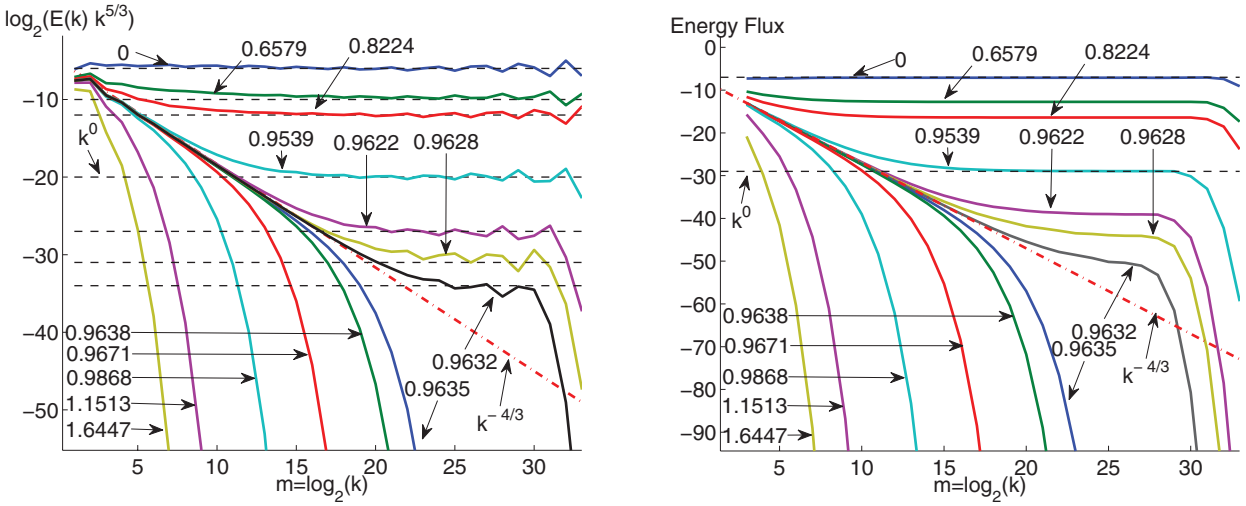

FIG. 1. (Color online) Numerical results for the energy spectrum (left) and the energy flux (middle) in the Sabra shell model for different values of γ.

in the following are highly nontrivial, justifying this study on its own right.

In Sec. II, we examine Eqs. (1) by means of a Sabra shell model. While shell models are admittedly an uncontrolled approximation to the full hydrodynamical equations (1) (for reasons briefly mentioned in the next section), we recall that they enjoy a distinguished status in the field of classical turbulence. In fact, they are regularly and widely used in this field as a convenient numerical tool that generally provides strong indications toward the correct spectra associated with the full hydrodynamic equations. This section presents numerical simulations that resolve the energy spectra $E_{\rm SM}(k)$ for different values of the mutual friction extending over an unprecedented range of wave vectors (see Fig. 1).We demonstrate that energy spectra depend crucially on the value of dimensionless mutual-friction frequency

$$\gamma \equiv \Gamma \big/ \varepsilon_0^{1/3} k_0^{2/3}, \tag{3}$$

which is normalized by the energy influx ε_0 at the outer wave vector k_0. There is a critical value $\gamma_{\rm cr} \approx 1$ at which $E(k) = E_{\rm cr} \propto k^{-3}$. For $\gamma < \gamma_{\rm cr}$, one has supercritical spectra $E_{\rm sp}(k) > E_{\rm cr}$ (at the same values of ε_0 and k_0) with Kolomogorov-41 (K41) tail $E_{\rm sp}(k) \simeq \epsilon^{2/3} k^{-5/3}$ and smaller energy flux $\varepsilon < \varepsilon_0$. For $\gamma > \gamma_{\rm cr}$, one has subcritical spectra $E_{\rm sb}(k) < E_{\rm cr}$ that terminate at final k.

To increase our trust in this complex behavior, we reanalyze (in Sec. III) the same basic Eqs. (1) analytically, using approximate differential closures for the energy flux over scales. These studies culminate with analytical solutions (10) and (13) for the supercritical and subcritical energy spectra, respectively. The closure techniques are not exact either, but we will see that they agree very well with the results of the shell model. The analytical spectra for $E_{\rm sp}(k)$ and $E_{\rm sb}(k)$ are shown in Fig. 2, where the stars correspond to the numerical data from Sabra shell model with similar values of the ratio $\gamma/\gamma_{\rm cr}$. One sees very good qualitative agreement between numerical and analytical results, despite the fact that both approaches are (uncontrolled) approximations of a very different nature. We propose that our results for the energy spectra can be considered as valid predictions on a semiquantitative level. A detailed analysis of our results is presented in the final Sec. IV.

II. SUPERFLUID ENERGY SPECTRA IN SHELL MODELS

Here, we investigate the superfluid energy spectra numerically in the shell-model approximation. Competing methods, such as vortex filament simulations or the solution of the nonlinear Schrödinger equation, are extremely demanding computationally, having therefore a very short span of scales. Shell models offer an attractive alternative, as recently suggested by Wacks and Barenghi,[8] who proposed a two-fluid shell model for superfluid turbulence using a Gledzer-Ohkitani-Yamada (GOY) shell model[9,10] with additional coupling terms. While only 18 shells were used in Ref. 8, we have been able to expand the range of scales quite significantly by increasing the number of shells to 36. This improvement allows us to probe an inertial interval over scales that extend to more than five decades, thereby making it possible to resolve subregions with different scaling behavior. Also, instead of using a GOY model, which suffers from the artifact of "period-three" oscillations in the energy spectrum, we used the Sabra shell model[11] in which this nonphysical phenomenon is removed and the scaling behavior becomes more transparent. These improvements allow us to get important additional information about the statistical behavior of superfluid turbulence.

A. "General" shell models of hydrodynamic turbulence

Shell models of turbulence[9,10,12–14] are simplified caricatures of the equations of fluid mechanics (1a) in wave-vector representation: they mimic the statistical behavior of $\boldsymbol{k}$-Fourier components of the turbulent velocity field $\boldsymbol{u}(\boldsymbol{k},t)$ in the entire *shell* of wave vectors $k_m < k_{m+1}$ by only one complex *shell velocity* u_m. The integer index m is referred to as the shell index, and the *shell wave numbers* are chosen as a geometric progression $k_m = k_0 \lambda^m$, with $\lambda > 1$ being the shell-spacing parameter; often, one chooses $\lambda = 2$. The equation of motion

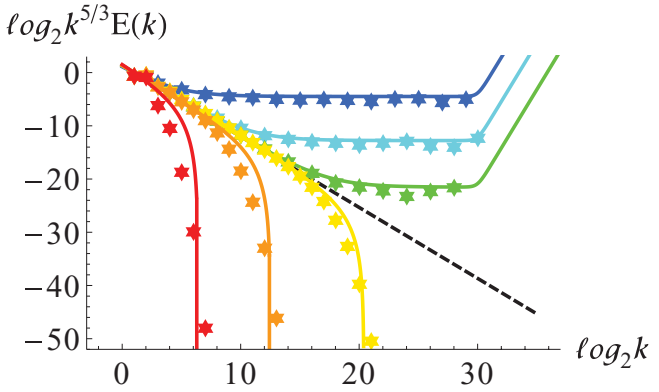

FIG. 2. (Color online) Analytical trial functions $E_{sp}(k)$ [Eq.(10)] and $E_{sb}(k)$ [Eq.(13)] in the differential energy-flux model. The stars show a comparison with data from the Sabra shell model at similar values of the ratio γ/γ_{cr}. The bottleneck effect $E_{sp}(k) \sim k^2$ at the highest wave vectors is removed from the Sabra shell model by proper choice of parameters to simplify the simulations.

of the fluid [e.g. Fourier transform of Eq. (1a)] is reduced to a dynamical equation of motion for $u_m(t)$:

$$\left[\frac{d}{dt} + \Gamma\right] u_m = \mathrm{NL}_m\{u_j\} + f_m. \tag{4a}$$

The model contains a time-independent mutual friction parameter Γ and random force terms f_m; the contribution of f_m as the energy influx at large scales is usually limited to the first few shells only. The nonlinear term $\mathrm{NL}_m\{u_j\}$, which originates from the $(\boldsymbol{v}\cdot\boldsymbol{\nabla})\boldsymbol{v}$ in Eq. (1a), should be (i) proportional to k_m (because of $\boldsymbol{\nabla}$), (ii) quadratic in the set of velocities $\{u_j\}$, and (iii) should conserve the total kinetic energy. In order to implement the Richardson-Kolmogorov idea of a step-by-step cascade energy transfer over scales, the set of the shell indices j in $\mathrm{NL}_m\{u_j\}$ should be localized around m. As as rule, one takes $j = m, m \pm 1, m \pm 2$.

B. Sabra shell model of turbulence

It is known that the original *GOY shell model*[9,10] suffers from nonphysical "period-three" oscillations of the energy spectrum that originate from artificial phase correlations in subsequent triads of the shell velocities. These oscillations were eliminated in the *Sabra shell model*[11] by a proper choice of the nonlinear term:

$$\begin{aligned}\mathrm{NL}_m\{u_j\} = i(&ak_{m+1}u_{m+2}u^*_{m+1} + bk_m u_{m+1}u^*_{m-1} \\ &- ck_{m-1}u_{m-1}u_{m-2}),\end{aligned} \tag{4b}$$

where * stands for complex conjugation and where the coefficients a, b, and c are real. Conservation of energy in the forceless inviscid limit requires that $a + b + c = 0$. It is known[9–14] that the statistical properties of the velocities in shell models mimic those of the three-dimensional hydrodynamic turbulence for $a = 1$, $b = c = -0.5$. In the forceless inviscid limit, the model has two quadratic invariants consisting of the energy E,

$$E = \sum_m E_m, \quad E_m \equiv \frac{|u_m|^2}{2}, \tag{5a}$$

and of a second quantity denoted H,

$$H = 2\sum_m \left(\frac{a}{c}\right)^m E_m. \tag{5b}$$

This last invariant is not positive definite and is loosely analogous to the helicity of a turbulent hydrodynamic flow.

The 1D turbulent energy spectrum $E(k)$ can be connected to E_m by the relation $E(k_m) = \langle E_m\rangle/k_m$. The energy flux over scales ε_m in the Sabra model is

$$\varepsilon(k_m) = 2\,\mathrm{Im}[ak_{m+1}S_{m+1} - ck_m S_m], \tag{5c}$$

where $S_m = \langle u_{m-1}u_m u^*_{m+1}\rangle$ is the third-order correlation function and Im[. . .] denotes imaginary part of [. . .].

It is clear from this description of the shell model that it only retains a "flavor" of the original fluid mechanics setting and that it constitutes an undeniably uncontrolled, and yet highly esteemed, approximation to the full hydrodynamical equations such as our Eqs. (1).

C. Numerical realization of the Sabra model

The set of $N = 36$ coupled Eqs. (4) was solved using fourth-order ETD-Runge-Kutta method[15] for stiff systems. In order to mimic the energy sink at very high wave numbers (e.g., due to Kelvin waves), a hyperviscosity term of the form $\nu k^4|u_m|^2$ with $\nu = 10^{-32}$ was added to the equation. For $c/a < 0$, which is our situation here, it is known that S_m exhibits period-two oscillations that are caused by the existence of a nonzero flux associated with the second invariant H. In order to remedy this complication, the energy pumping into the system was carried out by the "energy-only" forcing f_m (Ref. 11) in which the influx of the second invariant H was practically fully suppressed. In this way, we used random forcing (δ correlated in time), with a finite amplitude and a random phase in the first two shells, such that the forcing amplitudes are related to each other as $f_2 = \sqrt{-(c/a)}f_1$ and $f_1 = 0.01$. Following this protocol, the annoying period-two oscillations disappear, and one is free to study the behavior of the structure functions almost from the beginning of the inertial range. The mutual friction coefficient γ was chosen in the range $0 \leqslant \gamma < 1.65$ to expose the different solutions exhibited by the system. The use of hyperviscosity allowed us to maximize the extent of the inertial interval. However, the sharp onset of the viscous term leads to artificial oscillations in the energy spectra in a few shells around the dissipative cutoff (see Fig. 1, left panel). These oscillations are an artifact of the numerical procedure and not the result of the underlying dynamics.

Results of the numerical simulations of Sabra Eqs. (4), shown in Figs. 1 (continuous lines) and 2 (stars only), will be discussed in Sec. IV.

III. A DIFFERENTIAL MODEL FOR THE ENERGY SPECTRA

A. Energy balance equation with differential closure

The energy spectrum of pure hydrodynamic turbulence can also be studied analytically by investigating the energy balance equation

$$\frac{d\varepsilon(k)}{dk} + \Gamma E(k) = 0, \tag{6}$$

which is presented here in the stationary case [i.e., $\partial E(k)/\partial t \equiv 0$]. The energy density $E(k)$ is related to the total energy E by $E = \int E(k)dk$. Equation (6) directly follows from Eqs. (1) with some expression for the energy flux over scales $\varepsilon(k)$ in terms of the third-order correlation function of $\boldsymbol{u_k}$ exactly as in the case of classical turbulence. In order to proceed further, one can borrow a closure procedure from classical turbulence that expresses $\varepsilon(k)$ in terms of the energy spectrum $E(k)$. Even though this step is widely used, it is worth remembering that it is uncontrolled. The simplest *algebraic* closure relation suggested by Kovasznay,[16]

$$\varepsilon(k) \simeq \frac{5}{8}k^{5/2}E^{3/2}, \tag{7a}$$

just follows from K41 dimensional reasoning. The prefactor $\frac{5}{8}$ is chosen to simplify the appearance of some of the equations below. Notice that this simple algebraic approximation (7a) fails to include an important effect: the bottleneck energy accumulation near the intervortex scale ℓ. We therefore use the Leigh *differential* closure[17] for the energy flux in the form suggested by Nazarenko:[18]

$$\varepsilon(k) = -\frac{1}{8}\sqrt{k^{11}E}\frac{d}{dk}\left[\frac{E(k)}{k^2}\right]. \tag{7b}$$

Dimensionally, this closure relation coincides with Eq. (7a), but replaces $E(k)/k^3$ with $d[E(k)/k^2]/d\,k$. This allows one to account for the existence of thermodynamic equilibrium when $\varepsilon(k) = 0$ and $E(k) \propto k^2$. The prefactor $-\frac{1}{8}$ is chosen to get a frictionless (i.e., with $\Gamma = 0$) K41 solution

$$E_{\text{K41}}(\varepsilon|k) \equiv C_{\text{K}}\varepsilon^{2/3}k^{-5/3}, \quad C_{\text{K}} = \left(\frac{24}{11}\right)^{2/3} \approx 1.68, \tag{8a}$$

with C_{K} numerically close to its experimental value.

B. Simplified solution for the energy spectra

In this section, we overview some simplified solutions for the energy spectra that will serve as building blocks for the general solution. An exact solution of Eqs. (6) with the differential closure (7b) was found in Ref. 18 in the case $\Gamma = 0$. We rewrite it as $E(\varepsilon|k) = E_{\text{K41}}(\varepsilon|k)\,T_{\text{eq}}(k)$ with

$$T_{\text{eq}}(k) \equiv [1 + (k/k_{\text{eq}})^{11/2}]^{2/3}. \tag{8b}$$

One can see that $E(\varepsilon|k)$ has a thermodynamic tail $E(k) \propto k^2$ for $k \gg k_{\text{eq}}$, as required. A preliminary analysis into how to account for the mutual friction term in the balance equation (6) was done in Ref. 7 by using the algebraical closure (7a) and three regimes were identified.

(i) "Critical" scale-invariant solution:

$$E_{\text{cr}}(k) = \frac{16}{25}\frac{\Gamma^2}{k^3} = \left(\frac{4\gamma}{5}\right)^2\frac{\varepsilon_0^{2/3}k_0^{4/3}}{k^3}. \tag{9a}$$

At the special value $\gamma = \gamma_{\text{cr}} = \frac{5^{2/3}}{2} \approx 1.46$, it is realized for any k. One sees that γ_{cr} is of the order of unity and that the corresponding dimensional Γ_{cr} is about the turnover frequency of the outer-scale eddies.

(ii) For $\gamma > \gamma_{\text{cr}}$, solutions become "subcritical" $E_{\text{sb}}(k) < E_{\text{cr}}(k)$ and vanish at some finite $k = k_{\text{cr}}$:

$$E_{\text{sb}}(k) \simeq E_{\text{cr}}(k)\,T_{-}(k), \quad T_{-}(k) \equiv \left(1 - \frac{k^{2/3}}{k_{\text{cr}}^{2/3}}\right)^2. \tag{9b}$$

(iii) When $\gamma < \gamma_{\text{cr}}$, the energy spectra become "supercritical" with $E_{\text{sb}}(k) > E_{\text{cr}}(k)$. For $k \ll k_{\text{cr}}$, these spectra are close to the critical one, and for $k \gg k_{\text{cr}}$ they develop a K41 tail parametrized by $\varepsilon_\infty < \varepsilon_0$:

$$E_{\text{sp}}(k) \simeq E_{\text{K41}}(\varepsilon_\infty|k)\,T_{+}(k),\ T_{+}(k) \equiv \left(1 + \frac{k_{\text{cr}}^{2/3}}{k^{2/3}}\right)^2. \tag{9c}$$

When $\gamma \to \gamma_{\text{cr}}$, $\varepsilon_\infty \to 0$ and $k_{\text{cr}} \to \infty$:

$$\varepsilon_\infty = \varepsilon_0(\gamma - \gamma_{\text{cr}})^2\,, \quad k_{\text{cr}} = k_0|\gamma - \gamma_{\text{cr}}|^{-2/3}. \tag{9d}$$

These simple solutions allow us to construct physically motivated approximate analytical solutions to Eqs. (6) and (7b). The accuracy of these solutions can be improved if necessary by introducing a correcting polynomial expansion to our trial energy spectra. However, for the purpose of the present discussion, it is sufficient to present only the most simple versions of the energy spectra, which are determined by physical considerations only.

Notice that with the differential closure (7b) the energy balance Eq. (6) has a scale-invariant critical solution (9a) at precisely the same value of γ_{cr}. Moreover, for $\gamma \lessgtr \gamma_{\text{cr}}$, there are subcritical and supercritical solutions $E_{\text{sb}}(k) < E_{\text{cr}}(k)$ and $E_{\text{sp}}(k) > E_{\text{cr}}(k)$, which we will discuss in the following.

C. Supercritical energy spectra

Detailed analysis of the differential energy balance Eqs. (6) and (7b) leads us to the following form of approximate supercritical energy spectrum for $\Gamma < \Gamma_{\text{cr}}$:

$$\begin{aligned} E_{\text{sp}}(k) &= E_{\text{K41}}(\varepsilon|k)\left\{\sqrt{T_{+}^2(k) + T_{\text{eq}}^2(k) - 1} - T_{\text{sp}}(k)\right\}, \\ T_{\text{sp}}(k) &\equiv \frac{8}{15}\left(\frac{11}{3}\right)^{1/3}\frac{\Gamma}{(\varepsilon\,k_{\text{eq}}^2)^{1/3}}\left(\frac{k}{k_{\text{eq}}}\right)^{7/6}. \end{aligned} \tag{10}$$

This solution is plotted in Fig. 2. The solution (10) is constructed from the building blocks $E_{\text{K41}}(\varepsilon|k)$, $T_{\text{eq}}(k)$, and $T_{+}(k)$ discussed above and given explicitly by Eqs. (8a), (8b), and (9c), respectively. This solution (10) has a simple physical interpretation, which will be clarified by spelling out the regions of k that possess different scaling behavior; these regions are separated by k_{cr} and k_{eq}:

(i) For $k \ll k_{\text{cr}}$, $T_{\text{eq}} \approx 1$, $T_{+} \approx (k_{\text{cr}}/k)^{4/3} \gg 1$, $T_{\text{sp}} \ll 1$:

$$E_{\text{sp}}(k) \approx C_{\text{K}}\frac{\varepsilon^{2/3}k_{\text{cr}}^{4/3}}{k^3}, \quad \varepsilon(k) \approx \frac{15\,\varepsilon}{11}\left(\frac{k_{\text{cr}}}{k}\right)^2, \tag{11}$$

i.e., the solution has the form close to critical.

(ii) For $k_{\text{cr}} \ll k \ll k_{\text{eq}}$: $T_{+}(k) \approx T_{\text{eq}}(k) \approx 1$, $T_{\text{sp}}(k) \ll 1$. Thus, in this region, one observes the K41 spectrum $E_{\text{K41}}(\varepsilon|k)$

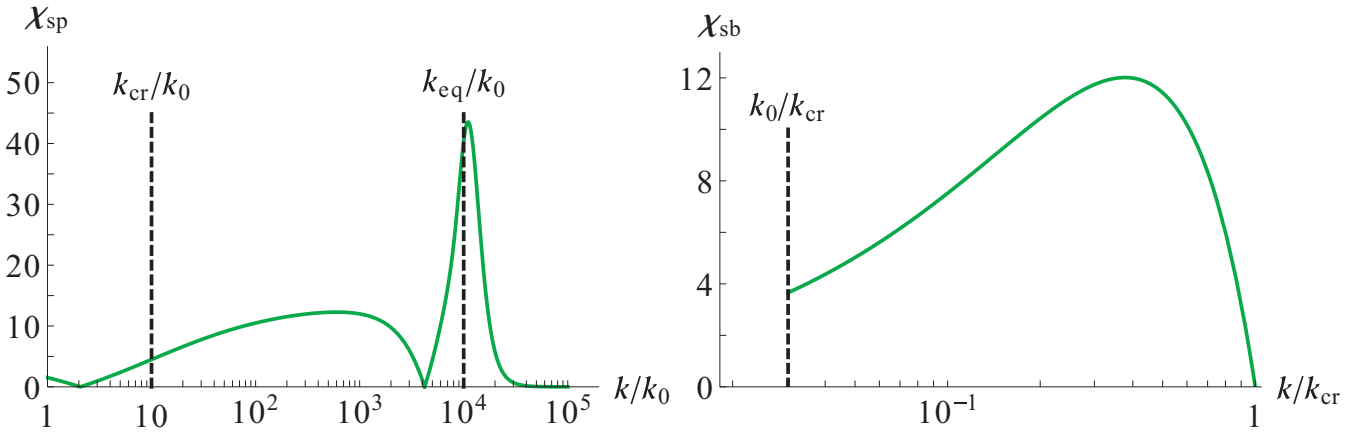

FIG. 3. (Color online) Mismatch functions χ_{sp} (resp. χ_{sb}) for the supercritical trial solution (resp. subcritical) defined in the text.

with the energy flux ε that is related to k_{cr} and Γ by the following global constraint:

$$\varepsilon - \varepsilon_0 = -\Gamma \int_{k_0}^{k_{eq}} E_{sp}(k)\, dk. \tag{12a}$$

Two other relations between these parameters are found from the boundary conditions for $E_{sp}(k)$ and $\varepsilon(k)$ at $k = k_0$. For example, from $\varepsilon(k_0) = \varepsilon_0$, one finds

$$\varepsilon_0 = \frac{15}{11}\left(\frac{k_{cr}}{k_0}\right)^2 \varepsilon. \tag{12b}$$

Notice that the square root in Eq. (10) is constructed such that for $k \gg k_{cr}$ $\sqrt{T_+^2 + T_{eq}^2 - 1} \approx T_{eq}$, thus ensuring that $E_{sp}(k)$ is close to the exact solution of Eqs. (6) and (7b) at $\Gamma = 0$, which predict the bottleneck energy accumulation for $k > k_{eq}$. This wave vector should be fixed by the boundary conditions at smallest possible scale in the problem, intervortex distance ℓ. This condition is outside of the scope of the present description, and currently we should consider k_{eq} as an external parameter. Finally, the $T_{sp}(k)$ term was obtained by performing an asymptotic analysis of the correction to the solution (10) when $\Gamma \neq 0$ and $k \gg k_{eq}$.

The accuracy of the trial solution $E_{sp}(k)$ can be quantified by introducing a mismatch function $\chi_{sp}(k) = 100 \times [\frac{d\varepsilon(k)}{dk} / \Gamma E_{sp}(k) - 1]$, which measures the percentage of error of $E_{sp}(k)$ when substituted into Eq. (6). As we can see in Fig. 3 (left panel), the disagreement never exceeds 15% except in the vicinity of k_{eq}, which has been left as an outside parameter here. Having in mind the approximate character of the differential approach, we conclude that our analytical form (10) for $E_{sp}(k)$ is a good approximation to the exact solution. Recall also that, if needed, our solution can be improved by supplementing it with appropriate polynomial corrections in the way demonstrated in Ref. 19.

D. Subcritical energy spectra

As $\gamma \to \gamma_{cr}$, the supercritical spectrum smoothly connects with the critical solution $E_{cr}(k)$ and indeed $k_{cr} \to +\infty$ as can be seen in Fig. 4. Eventually, we reach a point where $\gamma > \gamma_{cr}$ and the dissipation is so strong that the differential approximation predicts the resurgence of a finite wave vector k_{cr} such that the energy spectrum $E_{sb}(k_{cr}) = 0$ as well as the energy flux $\varepsilon(k_{sb}) = 0$ vanish. In this case, we propose the following form of approximate subcritical energy spectrum:

$$E_{sb}(k) = E_{cr}(k)\, T_-(k)\, T_{sb}(k), \quad T_{sb}(k) \equiv \left[1 - \frac{k^{3/4}}{k_{cr}^{3/4}}\right]^2. \tag{13}$$

This solution is plotted in Fig. 2. In addition to the building blocks already discussed above, this expression contains an extra correction $T_{sb}(k)$, which fixes its asymptotical behavior close to the terminal wave vector k_{cr}. Conservation of energy, in the form of the global constraint

$$\Gamma \int_{k_0}^{k_{cr}} E_B(k) dk = \varepsilon_0 \tag{14}$$

selects the value of k_{cr}, the evolution as a function of Γ of which can be seen in Fig. 4. When $\Gamma \to \Gamma_{cr}$, the position of the terminal wave vector is pushed to $k_{cr} \to +\infty$, which is consistent with a smooth connection with the critical solution $E_{cr}(k)$. On the other hand, when the dissipation is very strong $\Gamma \gg \Gamma_{cr}$, the terminal wave vector rapidly decreases and approaches $k_{cr} \to k_0$ asymptotically as it should.

The accuracy of the trial solution $E_{sb}(k)$ can be assessed by defining a mismatch function χ_{sb} in complete analogy with that defined in the previous paragraph. We can see in Fig. 3 (right panel) that the error always stays below 12%. This observation leads us to the conclusion that $E_{sb}(k)$ is a good analytical approximation to the exact solution, which is more than satisfactory for our purposes.

IV. DISCUSSION AND CONCLUSIVE REMARKS

A. Numerical versus analytical energy spectra

The main results of our numerical simulations in the framework of the Sabra shell model are presented in Fig. 1. In order to continue our discussion, notice that in the left panel, one sees a horizontal line for $\gamma = 0$ in the plots of $k^{5/3}E(k)$ versus k. Clearly, a K41 energy spectrum $E(k) \propto \varepsilon_0^{2/3} k^{-5/3}$ and k-independent energy flux $\varepsilon(k)$, which

is equal to the energy influx ε_0 (shown in right panel), is expected in this case. Intermittency corrections are practically invisible.

For small values of mutual friction parameter γ, we see that the energy flux first decays in the region of small k before approaching ε_∞, the value of which is analytically estimated by Eq. (9d). This behavior can be understood quite straightforwardly. Indeed, while the mutual damping frequency Γ is k independent, the K41 eddy-lifetime frequency increases as $\omega(k) \simeq \varepsilon^{1/3}k^{2/3}$. Therefore, it is always the mutual damping that must dominate the energy flux over scales in the region of small k. Such a damping naturally results in a decay of $\varepsilon(k)$. On the other hand, in the region of large k, it is the characteristic frequency of energy transfer over scales $\omega(k)$ which dominates over Γ and therefore the mutual friction can be neglected. In this region, $\varepsilon(k) \to \varepsilon_\infty$ and the K41 scaling $E(k) \propto \varepsilon_\infty^{2/3}$ must be recovered as is indeed confirmed both by the numerical and analytical plots of $E(k)$ in the left and middle panels.

Moreover, physical intuition [supported by Eq. (9d)] tells us that for some (critical) value of γ, the asymptotical value $\lim_{k\to\infty} \equiv \varepsilon_\infty$ should vanish. In this *critical regime*, the mutual damping frequency Γ is balanced by the cascade frequency $\omega(k)$, which can be estimated as $k\sqrt{kE(k)}$. This immediately suggests that $E_{\rm cr}(k) \simeq \Gamma^2/k^3$, which is corresponding precisely to our numerical observations (dashed red line in left panel) as well as our analytical predictions [Eq. (9a)].

Finally, we conclude by pointing out that the numerical value of $k_{\rm cr}$ is expected to be very sensitive to γ in the vicinity of $\gamma_{\rm cr}$ as hinted at by Eq. (9d). Indeed, the complete evolution of $k_{\rm cr}$ in both supercritical and subcritical regimes is presented in Fig. 4. Furthermore, we would like to mention that the existence of $k_{\rm cr}$, possibly much smaller than $1/\ell$ in the case of subcritical spectra, is not in contradiction with the coarse-grained approximation (1) for the description of the large-scale motions experienced by the underlying vortex-line tangle characteristic of quantum turbulence. It only means that the vortex lines are correlated with each other into a vortex bundle for distances $1/k_{\rm cr} \gg \ell$, and that vortex bending at scales below $1/k_{\rm cr}$ is suppressed. The simplest possible example of such superfluid flow can be realized in a cylindrical container, which undergoes an almost solid-body superfluid rotation. In this case, the quantum vortices are all approximately parallel to each other and there is no turbulent motion at intervortex distances. Nevertheless, despite the absence of an energy flux at scales $\sim 1/\ell$, a macroscopic turbulent state can be maintained. This analogy suggests that, in principle, the subcritical spectra when γ is large are not necessarily unphysical.

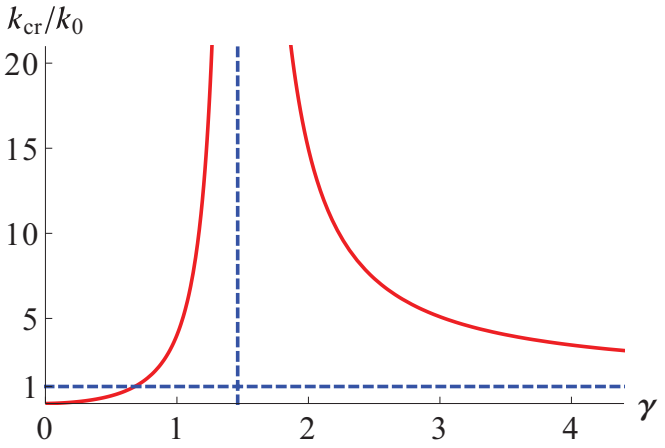

FIG. 4. (Color online) Evolution of the position $k_{\rm cr}$ as a function of the strength of the dissipation parameter. The vertical dashed line corresponds to $\Gamma \equiv \Gamma_{\rm cr}$ and the horizontal dashed line represents $k_{\rm cr} \equiv k_0$.

B. Mutual friction parameters γ versus α

The transition from subcritical to supercritical energy spectra is controlled by the dimensionless parameter γ instead of the more experimentally accessible mutual friction parameter α. Both parameters are temperature dependent (see Ref. 20 for a table of α versus T) and they can be related to each other by Eqs. (2) and (3). Notice, however, that unlike $\gamma_{\rm cr} \simeq 1$, which is universal, the critical value $\alpha_{\rm cr}$ does depend on experimental parameters such as the energy injection rate at the outer scale l_0 and on the extent of the "classical" inertial interval l/ℓ. It is nevertheless interesting to estimate $\alpha_{\rm cr}$ on the basis of typical experimental parameters. By substituting the critical solution (9a) in Eq. (2), one gets

$$\alpha_{\rm cr} \simeq \frac{5}{4\sqrt{2\ln(k_0\ell)}} \simeq \frac{0.9}{\sqrt{\ln(k_0\ell)}}. \tag{15}$$

With $k_0\ell \simeq 10^3$,[21] this gives $\alpha_{\rm cr} \simeq 0.34$. For $\alpha \ll \alpha_{\rm cr}$, one can neglect the effect of the mutual friction and directly substitute the K41 spectrum (8a) into Eq. (2). Under the assumption that this spectrum is valid up to $k \simeq 1/\ell$, one finds a remarkably simple relation for small α:

$$\gamma \simeq 2.25\,\alpha. \tag{16}$$

One should be mindful that due to the possible bottleneck energy accumulation,[22] which depends on the ratio of ℓ to vortex-core radius, the numerical coefficient in Eq. (16) can increase. Notwithstanding these reservations, we believe that this equation should be useful, even if only as a rough estimate.

C. The road ahead

To finish the discussion, we should underline again the approximations that will have to be relaxed in future work:

(i) The first one is the neglect of the turbulent motion of the normal component. We can study this approximation numerically, using a properly generalized[8] Sabra shell model,[11] and analytically, within properly formulated differential approximation for the normal and superfluid energy fluxes.

(ii) Second, using the two-fluid results, we will generalize the model of Ref. 22 of gradual eddy-wave crossover to the case of nonzero temperatures to study the effect of temperature suppression of the bottleneck energy accumulation near intervortex scales.

(iii) Lastly, we did not consider stability; the analysis of the stability of one- and two-fluid energy spectra against thermal perturbations should be accomplished, having in mind the possible self-sustained oscillations around, or in the vicinity of, stationary solutions.

ACKNOWLEDGMENTS

This work was supported by the EU FP7 Microkelvin program (Project No. 228464) and by the US Israel Binational Science Foundation.

[1]L. Landau, J. Phys. USSR **5**, 71 (1941) [Zh. Eksp. Teor. Fiz. **11**, 592 (1941)].
[2]S. Balibar, J. Low Temp. Phys. **146**, 441 (2007).
[3]M. S. Paoletti and D. P. Lathrop, Annu. Rev. Condens. Matter Phys. **2**, 213 (2011).
[4]W. Vinen and R. J. Donnelly, Phys. Today **60**(4), 43 (2007).
[5]M. A. Black, H. E. Hall, and K. Thompson, J. Phys. C: Solid State Phys. **4**, 129 (1971).
[6]W. F. Vinen, Phys. Rev. B **71**, 024513 (2005).
[7]V. L'vov, S. Nazarenko, and G. E. Volovik, JETP Lett. **80**, 535 (2004) [Pis'ma v ZhETP **80**, 546, (2004)].
[8]D. H. Wacks and C. F. Barenghi, Phys. Rev. B **84**, 184505 (2011).
[9]E. B. Gledzer, Dokl. Akad. Nauk SSSR **209**, 1046 (1973) [Soviet Physics Docl. **18**, 216 (1973)].
[10]M. Yamada and K. Ohkitani, J. Phys. Soc. Jpn. **56**, 4210 (1987).
[11]V. S. L'vov, E. Podivilov, A. Pomyalov, I. Procaccia, and D. Vandembroucq, Phys. Rev. E **58**, 1811 (1998).
[12]M. H. Jensen, G. Paladin, and A. Vulpiani, Phys. Rev. A **43**, 798 (1991).
[13]D. Pissarenko, L. Biferale, D. Courvoisier, U. Frisch, and M. Vergassola, Phys. Fluids A **5**, 2533 (1993).
[14]R. Benzi, L. Biferale, and G. Parisi, Phys. D (Amsterdam) **65**, 163 (1993).
[15]S. M. Cox and P. C. Matthews, J. Comput. Phys. **176**, 430 (2002).
[16]L. Kovasznay, J. Aeronaut. Sci. **15**, 745 (1947).
[17]C. Leith, Phys. Fluids **10**, 1409 (1967).
[18]C. Connaughton and S. Nazarenko, Phys. Rev. Lett. **92**, 044501 (2004).
[19]L. Boué, J. Laurie, V. L'vov, S. Nazarenko, and I. Procaccia (unpublished).
[20]R. J. Donnelly and C. F. Barenghi, J. Phys. Chem. Ref. Data **27**, 1217 (1998).
[21]P. M. Walmsley, A. I. Golov, H. E. Hall, A. A. Levchenko, and W. F. Vinen, Phys. Rev. Lett. **99**, 265302 (2007).
[22]V. L'vov, S. Nazarenko, and O. Rudenko, J. Low. Temp. Phys. **153**, 140 (2008).